Phase Transition of Thin-Film Superconducting Cylinders in a Magnetic Field. II. Angular Dependence*

R. Meservey
Francis Bitter National Magnet Laboratory, Massachusetts Institute of Technology, Cambridge, Massachusetts 02139

and

L. Meyers‡
Boston University, Boston, Massachusetts 02215

(Received 3 May 1972)

The normal-superconducting phase boundary for a thin-film microcylinder was measured in a magnetic field $\vec{H}$ making an angle θ with the cylinder's axis. The depression of the transition temperature for small values of transverse field H_t was proportional to H_t^2 as predicted by Tinkham, and equaled the predicted magnitude. At larger values of H_t there was a sudden discontinuity of slope in the T_c-vs-H^2 curve at a critical value of the transverse field H_{tc}. This discontinuity in slope apparently corresponds to a change from a superconducting state with uniform field penetration in the transverse direction to one with a single row of transverse vortices, the transverse-angular-momentum quantum number of the carriers changing from 0 to 1. A peculiar splitting of the flux-quantization resistance maxima was observed in the neighborhood of H_{tc} and qualitatively explained.

I. INTRODUCTION

Paper I[1] reported measurements of the phase boundary between the normal and superconducting states for thin-film superconducting hollow cylinders of micron size. The transition temperature was measured as a function of the magnetic field applied parallel to the axis of the cylinder. The results agreed well with Tinkham's theory[2] of the transition temperature in a parallel field. In Paper II we now report measurements of the phase boundary in which the effect of the angle between the axis of the cylinder and the magnetic field is investigated. A theory predicting the angular dependence of the transition temperature was briefly suggested by Tinkham[2] in explaining some of the earliest results by Little and Parks[3] on micron-sized hollow cylinders.

II. THEORY

A theory for the transition temperature of a small cylindrical thin-film superconductor in a magnetic field has been given by Tinkham.[2] This theory was briefly summarized in Paper I[1]; the main result is the prediction that the variations of the transition temperature can be described by the expression

$$\Delta T_c(H,\theta)=\frac{T_c(0)R^2}{8\lambda^2(0)H_{cb}^2(0)}\left[\left(H\cos(\theta)-\frac{n\phi_0}{\pi R^2}\right)^2+\frac{1}{3}\frac{d^2}{R^2}H^2\cos^2(\theta)+4H^2\sin^2(\theta)\right]. \quad (1)$$

Here θ is the angle between the axis of the cylinder and the magnetic field; R is the radius of cylinder; d is the thickness of thin-film cylinder; H is the magnitude of the applied magnetic field; n is the quantum number of the angular-momentum state; $\lambda(0)$ is the penetration depth of the film at $T=0$; $H_{cb}(0)$ is the thermodynamic critical field of the film material when in bulk form; $T_c(0)$ is the superconducting transition temperature for $H=0$; and $\Delta T_c(H,\theta)=T_c(\vec{H},\theta)-T_c(0)$ is the depression of T_c as a function of H and θ.

Equation (1) is derived by considering the Gibbs free energy of a superconductor as postulated by the Ginzburg-Landau theory,[4,5] which can be written in the form

$$G_s=G_n\int_{\substack{\text{vol of}\\ \text{supercond}}}d\vec{r}\left[\alpha|\psi(\vec{r})|^2+\tfrac{1}{2}\beta|\psi(\vec{r})|^4+(\hbar^2/2m^*)|\nabla|\psi(\vec{r})||^2+\tfrac{1}{2}|\psi|^2m^*V_s^2\right]+\int_{\text{all space}}d\vec{r}\left[\tfrac{1}{2}\mu(\vec{r})|\vec{H}(\vec{r})-\vec{H}_0(\vec{r})|^2\right]. \quad (2)$$

G_n is the Gibbs free energy of the cylinder in the normal state. G_s is a functional which when minimized with respect to ψ, and $\vec{A}$ gives the equilibrium Gibbs free energy. $\psi(r)$ is the order parameter and $|\psi(\vec{r})|^2$ is interpreted as the number of superconducting carriers of mass m^* and charge e^*. The velocity operator $\vec{V}_s$ is a function of the magnetic vector potential $\vec{A}$ and the phase Φ of the order parameter ψ,

$$\vec{V}_s=(1/m^*)\left[\hbar\nabla\Phi(\vec{r})-e^*\vec{A}(\vec{r})\right]. \quad (3)$$

In deriving and applying Eq. (1) it must be kept clearly in mind that we are dealing only with the limit in which $T\to T_c(H,\theta)$, the transition tempera-

ture for a given magnetic field and angle. $T_c(H,\theta)$ marks a second-order phase transition (by assumption in the Ginzburg-Landau theory) and for such a transition the order parameter ψ decreases continuously to zero as the temperature approaches T_c from below (H and θ constant). Thus, as we approach the phase boundary at T_c as defined by Eq. (1), the density of superconducting carriers $|\psi|^2$ approaches zero.

In this limit there can be a velocity field $\vec{V}_s$ of the superconducting carriers but no diamagnetic currents, since the current density $\vec{J}_s = |\psi|^2 e^* \vec{V}_s$ will approach zero because the carrier density $|\psi|^2$ approaches zero. No diamagnetic currents imply no distortion of the applied uniform magnetic field, and it is this geometrical simplicity that makes the problem tractable. This simplification is reflected in Eq. (2) by the disappearance of the last integral since $|\vec{H}(\vec{r}) - \vec{H}_0(\vec{r})|$ is proportional to the induced current density $\vec{J}_s$ at any value of $\vec{r}$ in the cylinder. This is fortunate, since this integral is over all space, not just the volume of the superconductor, and would not lead to the local Ginzburg-Landau equations.

The requirement that we consider only the limit of $T \to T_c$ avoids another difficulty. As $T \to T_c$ the characteristic length over which the order parameter can change from 0 to $|\psi|^2$ with an associated energy/unit volume equal to $|\alpha||\psi|^2$ is $\xi(T) = (\hbar^2/2m^*|\alpha|)^{1/2}$. When $T \to T_c$, $\xi(T) \to \infty$ as $(T_c - T)^{-1/2}$. This means that the energy associated with the gradient term over a sample of dimension L will be $[L/\xi(T)]^2$ times the energy associated with the $\alpha|\psi|^2$ term. When the characteristic dimension of the sample $L \ll \xi(T)$, we can neglect the gradient term, and since $|\psi|^2$ is uniform over the superconductor we can write the Gibbs free energy (per unit volume) as

$$G_s = G_n + \alpha|\psi|^2 + \tfrac{1}{2}\beta|\psi|^4 + \tfrac{1}{2}|\psi|^2 m^* \langle V_s^2 \rangle_{\text{av}} . \quad (4)$$

The condition $L \ll \xi(T)$ is certainly met when the characteristic dimension is the film thickness. When the characteristic dimension is the perimeter $2\pi R$, this condition will no longer hold for some value of H greater than zero. At this point the validity of Eq. (4) will be questionable.

The vastly simplified expression for the free energy, Eq. (4), is now minimized with respect to $|\psi|^2$ and the limit of $|\psi|^2 \to 0$ taken. This results in the condition

$$-\alpha = \tfrac{1}{2} m^* \langle V_s^2 \rangle_{\text{av}} . \quad (5)$$

Equation (5) states the condition for the transition temperature in a magnetic field is that the kinetic energy of the superconducing pairs equals the pair binding energy. The above argument was made in detail because, particularly for a transverse magnetic field, it may not be intuitively obvious that in the limit of $T = T_c$ the kinetic energy of the carriers is finite but there is *no* distortion of the applied field by diamagnetic currents. The validity of this picture is strongly supported by the experiments described in Paper I.

After disregarding the magnetic field energy we have to consider only the kinetic energy of the carriers. The velocity field can be found from the fluxoid-quantization condition. This condition, given by Eq. (6) follows from Eq. (3) and the fact that ψ is a single-valued function:

$$\oint m^* \vec{V}_s \cdot d\vec{l} + (e^*/c) \int\int \vec{H} \cdot d\vec{s} = nh . \quad (6)$$

Equation (6) is applied to any contour within the superconductor, and the second integral for the flux is over the surface enclosed by the contour. $\vec{H}$ is the applied magnetic field (which in the present experiments is uniform), and n is an integer or zero. Knowing $\vec{V}_s$ we find that for a cylindrical superconductor the kinetic energy per carrier as a function of radius r is

$$\tfrac{1}{2} m^* V^2(r) = (n\Phi_0 - \pi r^2 H)^2 \Big/ \frac{8\pi^2 R^2 m^* c^2}{e^{*2}} . \quad (7)$$

The binding energy of a superconducting pair is

$$-\alpha = \frac{H_{cb}^2(T)}{4\pi|\psi|^2} = \frac{H_{cb}^2(T) e^{*2} \lambda^2(T)}{m^* c^2} , \quad (8)$$

where the last expression comes from the definition of the penetration depth λ

$$\lambda^2 \equiv m^* c^2 / 4\pi |\psi|^2 e^{*2} . \quad (9)$$

Finally, when we introduce the usual two-fluid empirical temperature dependences for H_c and λ in terms of $t = T/T_c$,

$$H_{cb}(T) = H_{cb}(0)(1 - t^2) , \quad (10)$$

$$\lambda(T) = \lambda(0)(1 - t^4)^{-1/2} , \quad (11)$$

Eq. (5) becomes

$$H_{cb}^2(0)\lambda^2(0)\left(\frac{\Delta T_c}{T_c}\right) = \frac{\langle (n\phi_0 - \pi r^2 H)^2 \rangle_{\text{av}}}{8\pi^2 R^2} . \quad (12)$$

Equation (1) follows from Eq. (12) by averaging in the radial direction (R = average radius) and neglecting higher-order terms. In Eq. (1) the first term in the parenthesis describes the periodic variation of T_c caused by the quantization of flux associated with the magnetic field parallel to the cylinder's axis. The second term gives the monotonic decrease in T_c because of the screening currents within the film caused by the parallel field. This term is equivalent to the Ginzburg-Landau expression for the (parallel) critical field of a thin film,

$$H_{c\parallel}(T) = \sqrt{24}\, H_{cb}(T)[\lambda(T)/d] . \quad (13)$$

The last term in Eq. (1) represents the monotonic

decrease of T_c caused by the component of the magnetic field perpendicular to the axis of the cylinder. This term was derived by Tinkham by assuming that for a small transverse magnetic field the velocity-field pattern is similar to that shown in Fig. 1(b). The motion is down one side of the cylinder, half around the cylinder at the end, and back up the other side. When the length of the cylinder $L \gg R$ we can neglect the end effects, and the fluxoid-quantization condition, Eq. (6), is at any angle ϕ,

$$m^* V_s 2L + (e^*/c) H \sin(\theta)\, 2R \sin(\phi) L = \nu h \ . \qquad (14)$$

Here ν represents the angular-momentum quantum number about an axis in the direction of the transverse field, $H_t = H \sin\theta$. When $\nu = 0$ the velocity field is given by

$$V_s = (e^*/m^* c) H \sin\theta\, R \sin\phi \ . \qquad (15)$$

If we square V_s and average it over the azimuthal angle ϕ we obtain

$$\langle V_s^2 \rangle_{\rm av} = (e^*/m^* c)^2 \tfrac{1}{2} (R^2 H^2 \sin^2\theta) \ . \qquad (16)$$

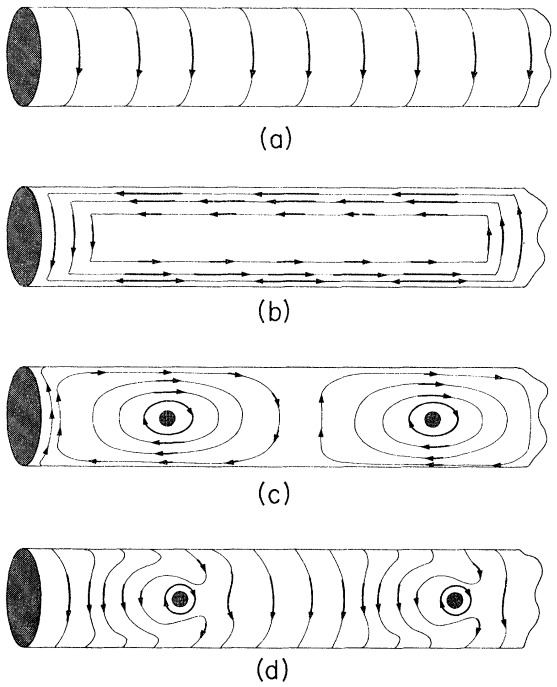

FIG. 1. Velocity fields (averaged over the film thickness) for the superconducting cylinder at the transition temperature for different applied magnetic fields. (a) Axial field only ($H_a \neq n\phi_0/\pi R^2$). (b) Small transverse field only. Superconducting carriers in zero-angular-momentum state. (c) Transverse field large enough to induce a single row of quantized vortices. (d) Sketch of the resultant velocity field for a combination of (a) and (c) resulting from a field $\vec{H}$ applied at an angle θ to the axis of the cylinder.

Substituting this into Eq. (5) and using as before Eqs. (8), (10), and (11) we obtain the depression of the transition temperature because of the transverse field:

$$\Delta T_c = T_c(0) R^2 H^2 \sin^2(\theta)/4 H_{cb}^2(0) \lambda^2(0) \ . \qquad (17)$$

Actually this term is one-half as large as the corresponding term in Eq. (1). This discrepancy results from Tinkham assuming a flat film $2R$ wide instead of a cylinder, the additional factor of $\frac{1}{2}$ coming from the average of $\sin^2\phi$ over the cylinder.

To use Eq. (1) to analyze the data we will mainly consider those points on the phase boundary for which $T_c(H, \theta)$ is a local maximum, and the first term in the parentheses of Eq. (1) is zero. We will assume that $\sin\theta = 0$ and $\cos\theta = 1$, which are sufficiently accurate approximations for the present measurements at small angles. With these assumptions Eq. (1) can be written as

$$T_c(0) - T_c(H, \theta) = \left(\frac{T_c(0) d^2}{24 \lambda^2(0) H_{cb}^2(0)}\right) H^2 \left(1 + \frac{12 R^2 \theta^2}{d^2}\right) \qquad (18)$$

or

$$T_c(0) - T_c(H, \theta) = \gamma_0 H^2 (1 + 12 R^2 \theta^2/d^2) \ . \qquad (19)$$

For $\theta = 0$ the depression of the transition temperature due to the finite thickness of the film is proportional to H^2 with a coefficient γ_0 which is characteristic of the cylinder. For a finite angle the coefficient of H^2 becomes

$$\gamma = \gamma_0 (1 + 12 R^2 \theta^2/d^2) \ . \qquad (20)$$

To compare with experimental data it is convenient to use the following expressions:

$$\gamma_0 = \left(\frac{-dT_c(H, 0)}{dH^2}\right)_{\theta=0} , \qquad (21)$$

$$\gamma_m = \left(\frac{-\partial T_c(H, \theta)}{\partial (H^2)}\right)_0 = \gamma_0 \left(1 + \frac{12 R^2 \theta^2}{d^2}\right) , \qquad (22)$$

$$\gamma = \frac{\partial}{\partial(\theta^2)} \left(\frac{-\partial T_c(H, \theta)}{\partial (H^2)}\right)_0 = \gamma_0 \frac{12 R^2}{d^2} \ . \qquad (23)$$

III. MEASUREMENTS

Experimental Procedure

The experimental procedure was described in detail in Paper I.[1] Thin-film microcylinders were prepared by vacuum evaporation of aluminum onto quartz fibers whose radii were in the neighborhood of 1 μ. A cylinder was mounted on a holder and immersed in liquid helium so that the cylinder was held parallel to the axis of a copper solenoid and at the midpoint of the solenoid. The axis of the cylinder could be tipped with respect to the magnetic field along two orthogonal axes. Measurements were made of the resistance of the cylinder as a function of the temperature T, the magnetic field $\vec{H}$, and the angle θ between $\vec{H}$ and

the axis of the cylinder (see Fig. 2). The transition temperature at zero magnetic field $T_c(0)$, was taken to be at the center of the steepest portion of the resistance-vs-temperature curve. The value of resistance at this point $R_{T_c}(0)$ was close to one-half the normal resistance. The phase boundary between the normal and superconducting state was then taken to be at those values of T, H, and θ which gave a resistance of $R_{T_c}(0)$.

The procedure was to first align the cylinder with the field by maximizing the transition temperature with respect to angle in a field of several hundred gauss. The position of alignment was easily recognized from a series of curves of resistance vs field such as shown in Fig. 3. Here we see the flux-quantization oscillations with their resistance minima outlining a quadratic background. At $\theta = 0$ the quadratic background is caused by the finite thickness of the films and agrees well with the theoretical value as was shown in Paper I. When the axis of the cylinder is tipped slightly from alignment, the curvature of the background parabola increases sharply with the angle θ. This is qualitatively the behavior expected from Eq. (1). It also justifies Tinkham's prediction of the extreme sensitivity of this background curve to field alignment. After the field was aligned by minimizing the background curvature, the temperature was raised above the transition temperature in zero field to eliminate possible trapped flux. Then starting at $T_c(0)$ with a sample resistance $R_{T_c}(0)$ and a given angle θ, the temperature was successively lowered and the value or values of H determined which gave a resistance $R_{T_c}(0)$ and therefore lay on the phase boundary. In some cases the magnetic field was held constant and the angle was varied to obtain points along the phase boundary. In none of the measurements was there noticeable hysteresis giving different values of the phase boundary when approached from different paths in (H, T, θ) space.

Results

Figures 4 and 5 show measurements of the transition temperature T_c as a function of the applied

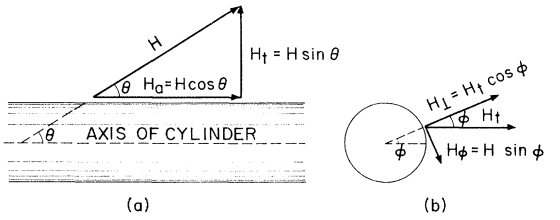

FIG. 2. Diagram defining the components of the magnetic field. (a) View perpendicular to the plane containing the axis of the cylinder and the applied magnetic field $\vec{H}$. (b) Axial view of the cylinder showing the components of the transverse field H_t.

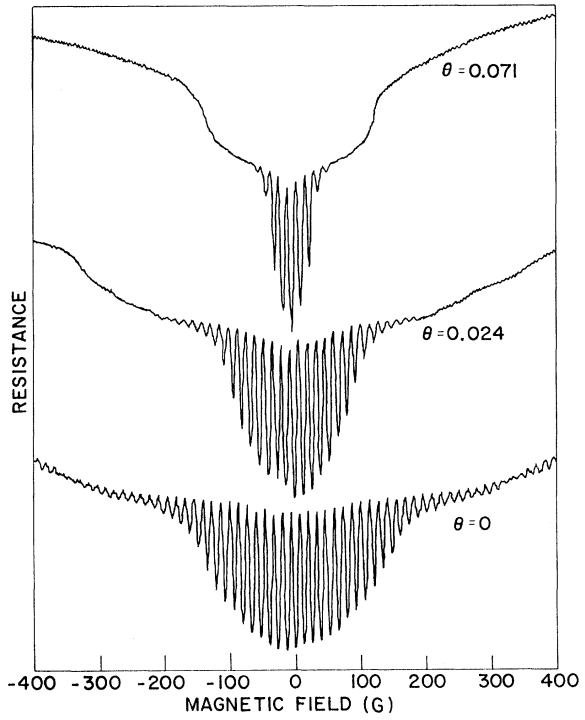

FIG. 3. Resistance of a superconducting aluminum cylinder at T_c as a function of the applied field H at different angles θ (in rad).

magnetic field $\vec{H}$ and the angle θ for a 2500-Å-thick Al film 1.397×10^{-4} cm in radius. In Fig. 4 the values of T_c plotted are the local maxima located at integral quantum numbers when the net circulation around the cylinder is zero. For $\theta = 0$ the decrease in T_c is accurately proportional to H^2 as expected from Eq. (19). For θ greater than zero, $(-dT_c/dH^2)$ increases with the angle. On close inspection it is seen that for each angle there are two regions of constant slope. The point at which the slope changes is indicated by the small arrows. Figure 5 shows the initial value of the slope $(-dT_c/dH^2)_0$ plotted against θ^2. It is seen that this plot is a straight line as predicted by Eq. (22). The dashed line is the theoretical value given by the right-hand side of Eq. (22), $\gamma_0(1+12R^2\theta^2/d^2)$, γ_0 being the background slope at $\theta = 0$. The fit is excellent, probably fortuitously close since the coefficient of θ^2 in Eq. (1) is supposed to be only approximate. But in any case the general behavior of this 2500-Å film at small fields is exactly as predicted. The break in the slope at some finite field was not predicted.

Figures 6–8 are similar measurements for a very thin Al film 340 Å thick and with a radius of 1.64×10^{-4} cm. Figure 6 again shows the quadratic dependence of T_c on H for $\theta = 0$. (The measured points were omitted since they are plotted in Fig.

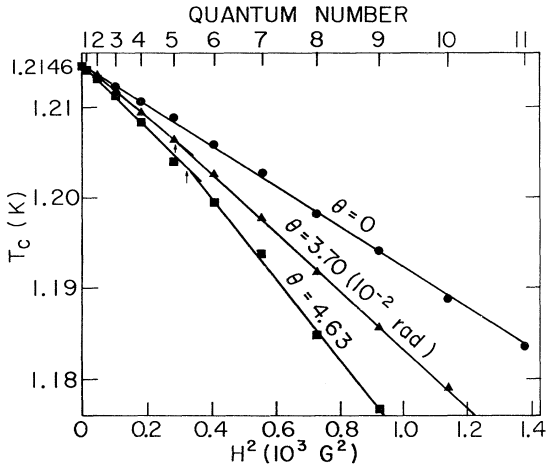

FIG. 4. T_c vs H^2 for three values of θ. Cylinder 5, thickness $d = 2500$ Å, radius $R = 1.40 \times 10^{-4}$ cm.

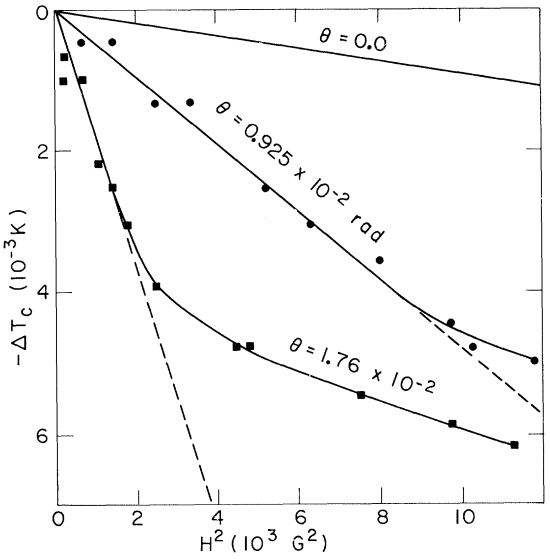

FIG. 6. Depression of T_c vs H^2 for three values of θ. Cylinder 1, $d = 340$ Å, $R = 1.64 \times 10^{-4}$ cm.

10 of Paper I.) The slope is very much less than in the 2500-Å film as we would expect. At finite angles we see a similar behavior to that of the thick film in which $-dT_c/dH^2$ is constant within the rather large scatter of the data up to some critical value of H at which there is a sudden break to a smaller value of $(-dT_c/dH^2)$. Figure 7 shows the data of Fig. 6 (with the addition of some data at a higher angle) replotted with the transverse field as the ordinate. This plot suggests that the transverse field is the pertinent variable in determining the initial slope $(-dT_c/dH^2)_0$. The break in slope occurs at a definite value of H_t, but for larger values of H_t another factor controls the variation of T_c. In Fig. 8 the initial values of the slopes $(-dT_c/dH^2)_0$ are plotted against θ^2. The results are quite scattered but agree with the dashed theoretical curve within a factor of 2. Actually the measurements on the 340-Å film contained considerable scatter which was partly correlated with structure in the resistance transition (see Paper I) and partly resulted from the decrease in magnitude of the effects in very thin films so that much greater accuracy in temperature control and measurement was required. The main new behavior introduced by the 340-Å film measurement is that the value of $(-dT_c/dH^2)$ beyond the break decreases rather than increases as in the case of the 2500-Å film.

Figure 9 shows the variation of T_c with H^2 for a number of different angles for a cylinder 1095 Å

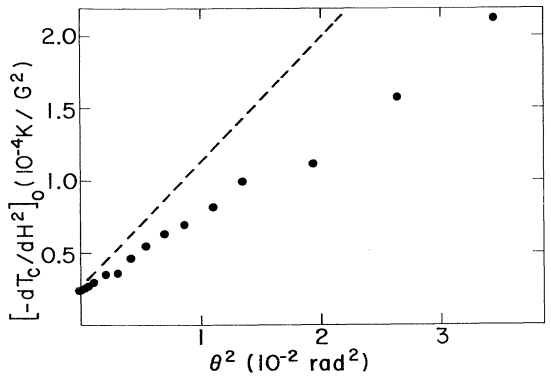

FIG. 5. $(-dT_c/dH^2)_0$ vs θ^2 (at small values of H) for cylinder 5. Dashed line is theoretical value.

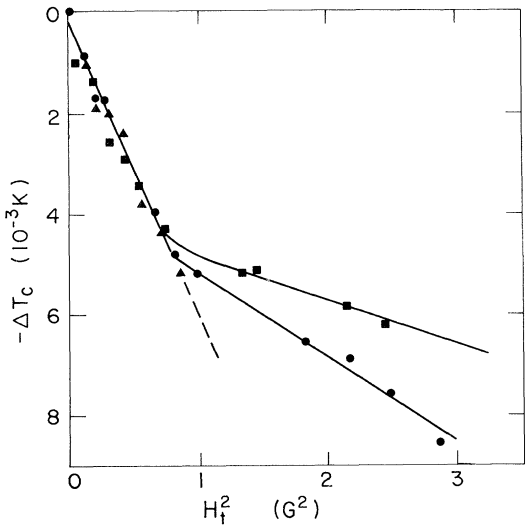

FIG. 7. Depression of T_c vs H_t^2 for cylinder 1.

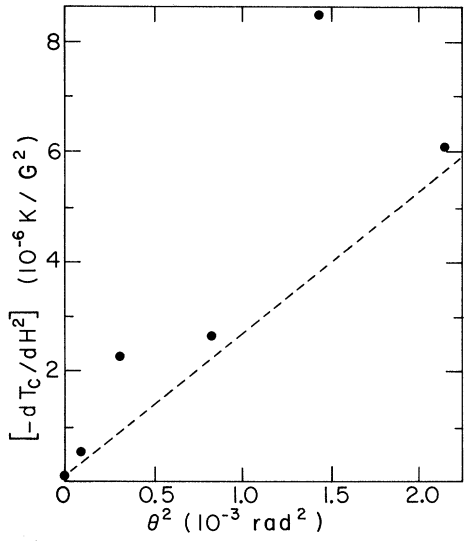

FIG. 8. $(-dT_c/dH^2)_0$ vs θ^2 (at small values of H) for cylinder 1. Dashed line is theoretical value.

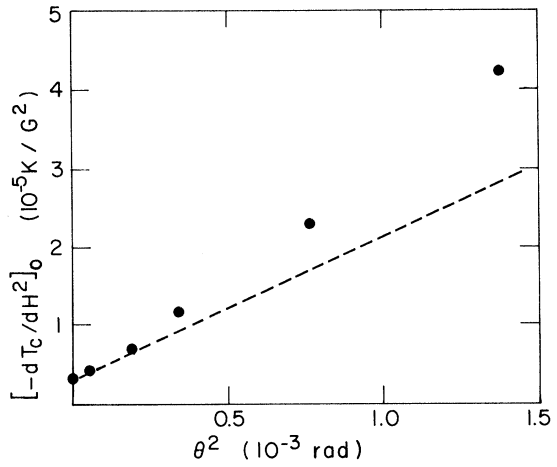

FIG. 10. $(-dT_c/dH^2)_0$ vs θ^2 (at small values of H) for cylinder 4. Dashed line is theoretical value.

thick and with a 2.50×10^{-4}-cm radius. The behavior is qualitatively very similar to the thinner film with two clearly defined regions of constant slope on the T_c-vs-H^2 plot. Figure 10 shows that $(-dT_c/dH^2)_0$ is approximately proportional to θ^2 although the coefficient is somewhat larger than the theoretical one. In Fig. 9 the slope $(-dT_c/dH^2)$ suddenly decreases at approximately the same value of the transverse field $H_t = 0.36$ G. This result is obtained from Fig. 11 if we neglect the point at the smallest angle. For somewhat higher values of field we have different values of the slope for each value of θ.

Figure 12 gives $(-dT_c/dH^2)_0$ as a function of θ^2 for a cylinder 1030 Å thick and 1.78×10^{-4} cm in radius. The result is not very different except that in this case the measured values are less than the theoretical.

Figures 13–15 gives results for a cylinder 320 Å thick and 1.08×10^{-4} cm in radius. The data for T vs H^2 for various angles are similar to the 1095-Å cylinder. In Fig. 14 the experimental values of $(-dT_c/dH^2)_0$ are in fair agreement with the theory. In Fig. 15 the values of the transverse field at which the break in slope appears in Fig. 13 are approximately 1.2 G except for the two smallest angles. For somewhat higher values of field we have different values of the slope for each value of θ.

For this sample an additional phenomenon was observed. As H was increased (see Fig. 16) it

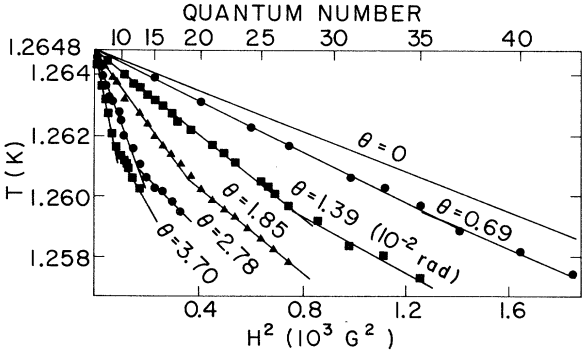

FIG. 9. T_c vs H^2 for six values of θ. Cylinder 4, $d = 1095$ Å, $R = 2.50\times10^{-4}$ cm.

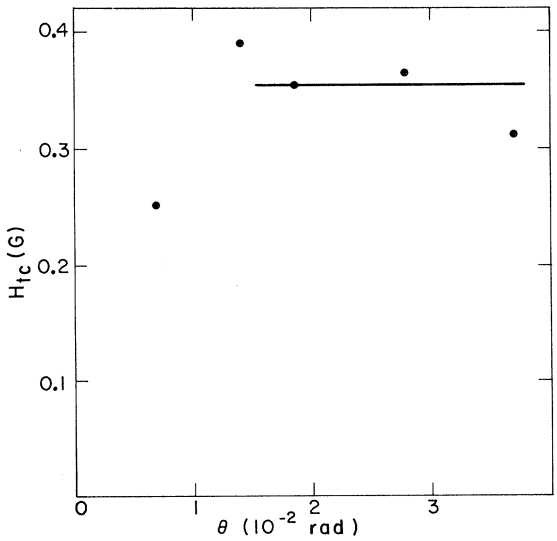

FIG. 11. Critical transverse field H_{tc} vs θ for cylinder 4.

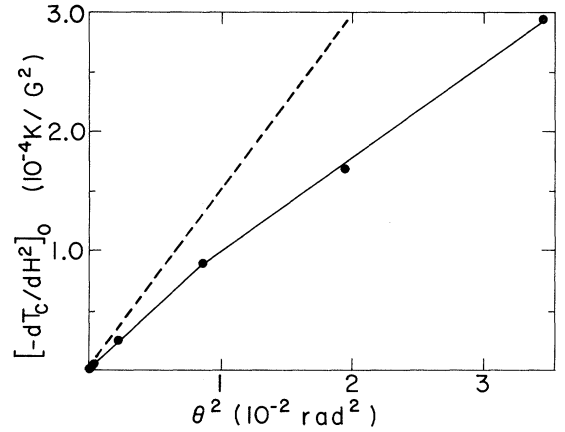

FIG. 12. $(-dT_c/dH^2)_0$ vs θ^2 (at small values of H) for cylinder 2. Dashed line is theoretical value.

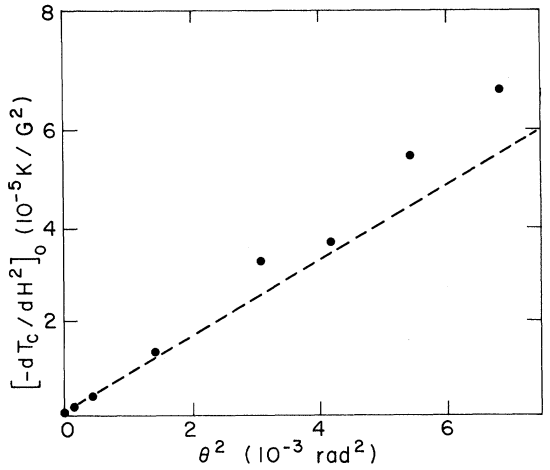

FIG. 14. $(-dT_c/dH^2)_0$ vs θ^2 (at small values of H) for cylinder 3. Dashed line is theoretical value.

was found that at a finite angle the flux-quantization resistance maxima were split. When $\theta = 0$ these maxima in the resistance as a function of H are in theory (and to a fair approximation in practice) the intersection of parabolas for different values of orbital angular momenta.

However, for a finite angle and for values of H greater than a certain value, a notch appears at the position of the resistance maxima. If we interpret this as a feature of the phase boundary, it reflects a sudden increase in the transition temperature near the values of field corresponding to half-integral values of flux quanta. As the field increases the depth of the notch and the splitting of the resistance peaks increases montonically. This splitting of the resistance peaks was also observed in cylinder 1, but in no others, which implies that a small film thickness may be necessary. The significance of this effect will be discussed in Sec. IV.

IV. DISCUSSION

For all five of the cylinders measured, the depression of T_c in a magnetic field was proportional to θ^2 for small values of θ, the angle between the axis of the cylinder and the field. Table I shows that the value of

$$\gamma_m = \frac{\partial}{\partial \theta^2}\left(-\frac{\partial T_c(H,\theta)}{\partial H^2}\right)_0$$

is approximately equal to the value predicted by Eq. (1) or Eq. (22). There seems to be no correlation between the deviations from the theory and the values of the thickness d and the radius R, and we can probably assume the scatter to be random.

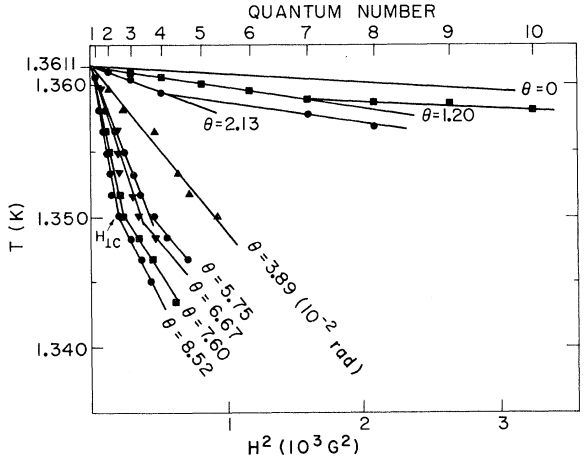

FIG. 13. T_c vs H^2 for eight values of θ. Cylinder 3, $d = 320$ Å, $R = 1.08 \times 10^{-4}$ cm.

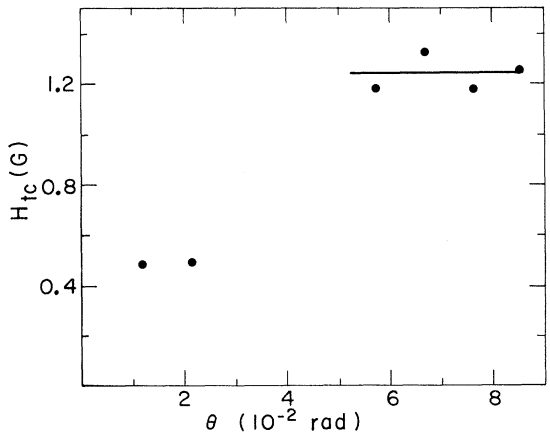

FIG. 15. Critical transverse field H_{tc} vs θ for cylinder 3.

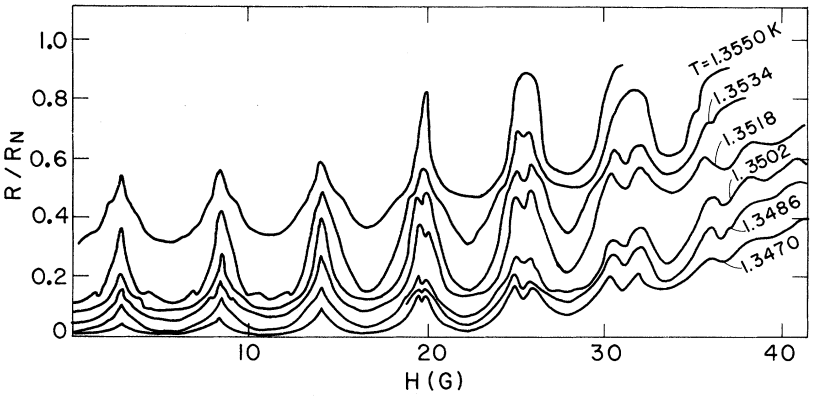

FIG. 16. Resistance of cylinder 3 (divided by normal-state resistance) as a function of the applied field at a series of temperatures near T_c for $\theta = 5.74\times10^{-2}$ rad. For $H \geq 20$ G the resistance maxima are split into two peaks whose separation increases with H.

The agreement with Eq. (1) is definitely better than with the presumably more exact Eq. (17).

When the depression of T_c is plotted against H^2 we obtain (for small values of H) a line of constant slope, the magnitude of the slope increasing with θ. Figures 9 and 13 show such results for cylinders 4 and 3. For $\theta > 0$ there is a discontinuity in slope at a certain value of the applied field for each value of θ. The value of the transverse field (H_{tc}) at which the discontinuity in slope occurred was found to be nearly the same for all but the smallest angles (see Figs. 11 and 15). The same behavior was observed in cylinders 1 and 5, although here only two values of angle had been used. In cylinder 2 the field applied was presumably too small to have reached the region of the discontinuity. This behavior immediately suggests the quantization of angular momentum in the transverse direction associated with the appearance of a row of vortices. At such a discontinuity the velocity field associated with H_t might change from that shown in Fig. 1(b) to something like that shown in Fig. 1(c). This corresponds to a change in the angular momentum of the supercarriers about a transverse axis from a quantum number $\nu = 0$ to $\nu = 1$. Figure 1(d) is an attempt to show the sort of velocity field obtained when the transverse vortex structure of Fig. 1(c) is superimposed on an azimuthal velocity field corresponding to an axial magnetic field.

This vortex state should have a second-order transition to the normal state, and its free energy should perhaps vary as H^2 because of the finite diameter of the superconductor. In Figs. 9 and 13 we notice that the slopes at higher values of H^2 when extended back to the T_c axis all lie in a small region of temperature except for the data for the smallest angles. This can perhaps be interpreted as the transition temperature for $\nu = 1$ at $H = 0$ and is below T_c for $\nu = 0$ and therefore not observed.

If this general picture is correct we should expect the $\nu = 1$ state to have a second-order transition to the normal state when one quantum of flux is contained in an area of about $2R\xi(T)$. The lateral dimension of the vortex is fixed by the diameter of the cylinder. The minimum distance between vortices should be about $\xi(T)$. From this simple model we would expect the critical transverse field to occur at

$$H_{tc} \approx \phi_0 / 2R\xi(T) \ . \tag{24}$$

The coherence distance $\xi(T)$ depends on T as

TABLE I. Summary of data on angular dependence of T_c in a magnetic field for small values of the angle θ.

Cylinder No.	Film thickness d (10^{-5} cm)	Magnetic field periodicity ΔH (G)	Cylinder radius R (10^{-4} cm)	$T_c(0)$[a] (K)	$\gamma_0 = (-dT_c/dH^2)_{\theta=0}$ (K/G^2)	$\gamma_m = \frac{\partial}{\partial\theta^2}\left(\frac{-\partial T_c(H,\theta)}{\partial H^2}\right)_0$ (K/G^2 rad^2)	$\gamma_t = \gamma_0 12R^2/d^2$ (K/G^2 rad^2)	γ_m/γ_t
1	0.34	2.45	1.64	1.3940	9.25×10^{-8}	0.48×10^{-2}	0.26×10^{-2}	1.85
2	1.03	2.07	1.78	1.2527	3.58×10^{-6}	0.93×10^{-2}	1.28×10^{-2}	0.73
3	0.32	5.70	1.08	1.3618	5.82×10^{-7}	0.95×10^{-2}	0.79×10^{-2}	1.20
4	1.095	1.03	2.50	1.2648	2.83×10^{-6}	2.66×10^{-2}	1.77×10^{-2}	1.50
5	2.50	3.38	1.40	1.2146	2.40×10^{-5}	0.51×10^{-2}	0.90×10^{-2}	0.57

[a]The absolute value of $T_c(0)$ is perhaps accurate to 10^{-3} K. The value given to a precision of 10^{-4} K is arbitrary and used only for consistency with relative values which are at least this precise.

TABLE II. Comparison of measured critical transverse magnetic field H_{tc} and theoretical value.

Cylinder No.	$2R$ (10^{-4} cm)	$(d\xi_0)^{1/2}$ [a] (10^{-5} cm)	θ (10^{-2} rad)	$\left(\frac{T_c}{T_c-T_{c_1}}\right)^{1/2}$	$D=\left(\frac{T_c}{T_c-T_{c_1}}\right)^{1/2}(d\xi_0)^{1/2}2R$ (10^{-7} cm^2)		ϕ_0/D (G)	H_{tc} (G)	$\frac{H_{tc}D}{\phi_0}$
1	3.28	2.33	0.925	18.7	1.43		1.45	0.89	0.61
			1.76	18.3	1.40		1.48	0.88	0.59
3	2.16	2.26	1.20	25.0	1.22		1.70	0.47	0.28
			2.13	30.0	1.46		1.42	0.49	0.35
			5.75	11.3	0.55		3.77	1.16	0.31
			6.67	11.1	0.54		3.84	1.28	0.33
			7.60	11.1	0.54		3.84	1.18	0.31
			8.52	11.1	0.54		3.84	1.23	0.32
4	5.00	4.18	0.64	20.4	4.27		0.48	0.24	0.50
			1.39	17.7	3.70		0.56	0.39	0.70
			1.85	17.1	3.58		0.58	0.35	0.60
			2.78	15.3	3.20		0.65	0.36	0.55
			3.70	15.1	3.16		0.66	0.32	0.49
5	2.80	6.30	3.70	10.0	1.75	1.75	1.18	0.63	0.53
			4.63	10.3	1.82	1.82	1.14	0.82	0.72

[a]It is assumed for Al that $\xi_0 = 1.6\times10^{-4}$ cm.

$$\xi(T) = \xi(0)\,[T_c/(T_c - T)]^{1/2}\,. \tag{25}$$

For thin films such as these with a short mean free path l, which is approximately equal to the thickness d, we have

$$\xi(0) \approx (\xi_0\, l)^{1/2} \approx (\xi_0 d)^{1/2}\,. \tag{26}$$

From Eqs. (24)–(26) we have

$$H_{tc} = \frac{\phi_0}{2R(\xi_0 d)^{1/2}\,[T_c/(T_c - T)]^{1/2}}\,.$$

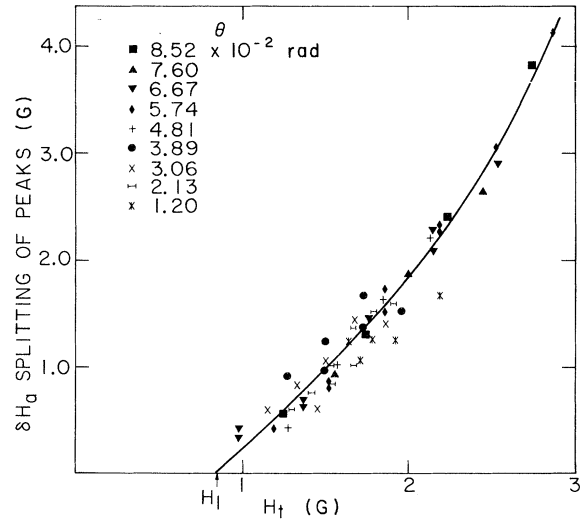

FIG. 17. Separation of the split peaks in the resistance versus H_t for the data in Fig. 16 and eight other values of θ. The splitting correlates well with H_t, and there is a threshold value of transverse field at approximately H_1, where the effect appears.

Table II gives the ratio of the measured to the predicted values of H_{tc} for cylinders 1, 3, 4, and 5. The results are rather consistent for each film even for small values of θ for which H_{tc} is considerably larger than for larger values of θ. The order of magnitude of the ratio in each case is fairly close to unity. The reasonably good agreement suggests that H_{tc} marks the transition from the $\nu = 0$ to a $\nu = 1$ vortex state with a single row of vortices. The 2500-Å-thick film (cylinder 5) does not entirely fit this picture since the magnitude of the slope $(-dT_c/dH^2)$ increases slightly instead of decreases. The explanation of this is not clear. For cylinder 3 there appears to be an additional discontinuity at a value of $H > H_{tc}$, although the results were not very reproducible. This perhaps corresponds to a vortex state with

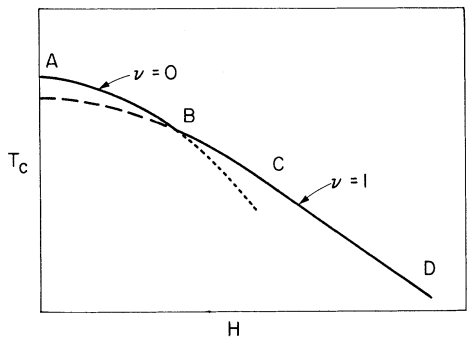

FIG. 18. Suggested form of the phase boundary for a singly connected film in a magnetic field $\vec{H}$ which has a transverse component. ν refers to the angular-momentum quantum number in the transverse direction.

a second row of vortices when $2R > \xi(T)$. For larger fields the dependence of T_c on H becomes linear and azimuthal flux quantization disappears. This behavior is characteristic of the two-dimensional vortex state.

The appearance of the $\nu = 1$ vortex state presumably explains the splitting of the resistance maxima observed in cylinder 3 (Fig. 16) and cylinder 1 (Fig. 20). It was found that if the splitting of the resistance maxima (measured in terms of the axial magnetic field) was plotted (Fig. 17) as a function of the transverse field H_t we obtain for all values of θ a nearly universal curve. This curve implies that H_t is the controlling factor in the splitting and that there is a threshold field (H_1 in Fig. 17) at which the effect appears. The value of $H_1 \approx 0.83$ G is slightly less than the value of $H_{tc} \approx 1.2$ G for the larger angles.

To try to explain this splitting of the resistance maxima let us assume that the effect is a thermodynamic one and that there is a corresponding splitting of the minima of T_c. This assumption is not necessary, but it is plausible. We know that the quadratic background and the parabolic flux-quantization oscillations are thermodynamic effects which are accurately reflected by the resistance. Furthermore, the splitting occurs at a discontinuity in the slope of the phase boundary which seems to coincide with the onset of the vortex state. These facts make it reasonable to try to explain the details of the splitting as a thermodynamic effect.

We will assume that the sudden change in slope at H_{tc} may be understood from Fig. 18, in which the transition temperature of the $\nu = 0$ and $\nu = 1$ states are plotted as a function of H, ignoring for the moment that the films are doubly connected and, therefore, suppressing the oscillations due to azimuthal flux quantization. T_c varies as H^2 from A to B. At B the single-line vortex state appears, and we assume that T_c varies with H^2 (or at least with a higher power of H than unity) but with a

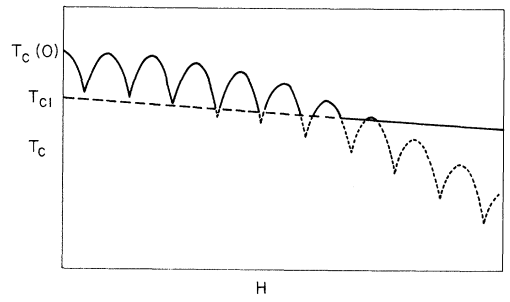

FIG. 19. Simplified diagram showing the $\nu = 0$ state with flux-quantization oscillations intersecting the $\nu = 1$ state drawn without oscillations.

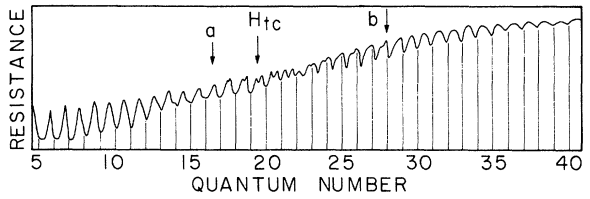

FIG. 20. Resistance vs applied magnetic field for cylinder 1. The quantum numbers correspond to values of the magnetic field giving integral numbers of flux quanta through the cylinder. The field period per quantum is 2.45 G. The splitting of the resistance peaks (corresponding to minima in T_c) starts at $n = 17$. Noticeable deviation from the initial slope in Fig. 6 is marked by the arrow at a; complete transition in the slope in Fig. 6 is shown by the arrow at b. H_{tc} determined from Fig. 6 is also marked.

smaller coefficient. From B to C the two-dimensional vortex state develops and from C to D, T varies as H, a characteristic of the two-dimensional vortex state. The region CD is observed experimentally at high fields after the quantization effect is no longer observed. In Fig. 19 we suggest a simplified picture of the intersection of the phase boundaries of the two states. The $\nu = 0$ state is represented as having flux-quantization oscillations. The $\nu = 1$ state is represented without oscillations for simplicity in presenting the essence of the argument. As T_c for the $\nu = 0$ state approaches T_c for the $\nu = 1$ state the minima of the phase boundary, corresponding to high values of azimuthal circulation, are the first to become unstable and switch to the $\nu = 1$ state. This switching could explain the progressive cutting off of the minima in T_c (maxima in resistance). Such an explanation is certainly not complete, a fact which is demonstrated by Fig. 20, the measured resistance-vs-magnetic-field curve at a given temperature for cylinder 1. The notch in the resistance peak (corresponding to a maximum in T_c) appears at quantum number $n = 17$. As n increases, the notch gets successively deeper and finally by $n = 30$ completely dominates the quantum oscillations in T_c. On Fig. 20 are marked the position of H_{tc} from Fig. 6 and the position a, where the initiation of the change in slope takes place in Fig. 6 and position b where the change in slope in Fig. 6 is essentially complete. Coincidence in the change in slope with the change in shape of the quantum oscillations shows quite conclusively that both effects have the same cause, presumably the transition from the $\nu = 0$ to the $\nu = 1$ state.

The vertical lines on Fig. 20 in the region from $n = 17$ to $n = 30$ are interpolations of the field at integral values of n as determined from $n < 17$ and $n > 30$. Judging by these equally spaced lines the position of the notch gradually changes from a

half-integral quantum position to an integral quantum position from $n = 17$ to $n = 30$. Also the shape of the quantum oscillations for the $\nu = 1$ state appears to be inverted from what they are in the $\nu = 0$ state. As yet we have no detailed explanation of this behavior.

*Research supported by the Office of Naval Research and the NSF.

†Supported by the NSF.

‡Present address: San Francisco State College, San Francisco, Calif. 94132.

[1]L. Meyers and R. Meservey, Phys. Rev. B 4, 824 (1971).

[2]M. Tinkham, Phys. Rev. 129, 2413 (1963).

[3]W. A. Little and R. D. Parks, Phys. Rev. Letters 9, 9 (1962).

[4]V. L. Ginzburg and L. D. Landau, Zh. Eksperim. i Teor. Fiz. 20, 1064 (1950).

[5]D. H. Douglass, Jr., Phys. Rev. 132, 513 (1963).

PHYSICAL REVIEW B VOLUME 6, NUMBER 7 1 OCTOBER 1972

Thermal Conductivity in the Two-Band Model of Superconducting Transition Metals Containing Nonmagnetic Impurities

Pramod Kumar and S. N. Gupta
Department of Physics, University of Roorkee, Roorkee, India
(Received 3 January 1972)

Using the Green's-function formulation, an expression has been derived for the thermal conductivity of transition-metal superconductors containing nonmagnetic impurities in the two-band model of Suhl, Matthias, and Walker (SMW). The calculations have been carried out neglecting the interband electron-phonon coupling and taking the interband-scattering collision time $\tau_{sd} \approx 10^{-12}$ sec. The thermal conductivity K is found to be the sum of two terms K_1 and K_2. K_1 is the dominating term and depends in a complicated manner on both energy gap parameters $\bar{\Delta}_s$ and $\bar{\Delta}_d$, due to s and d bands, respectively. On the other hand, K_2 depends only on $\bar{\Delta}_d$ and is smaller by a factor of $\sim 10^{-7}$. A log-log plot of thermal conductivity vs temperature turns out to be a straight-line curve with a slight change in its slope at a temperature which depends upon the impurity concentration. Furthermore, K is found to decrease with increase in impurity concentration. These qualitative features of the present study are in very good agreement with the recent experimental investigations of Anderson *et al.* on niobium and lend support to the validity of the SMW two-band-model theory.

I. INTRODUCTION

The two-band model was first proposed by Suhl, Matthias, and Walker[1] (SMW). They showed that at low temperatures both the s-band and d-band electrons in the transition metals can be in the superconducting phase. Some recent experimental investigations also show evidence for the existence of a second energy gap,[2,3] and this has given rise to great interest in the study of this model. Thus there have been several theoretical investigations[4–8] within the framework of this model. It has been found that this model quite successfully explains various physical properties of superconducting transition metals. Chow,[5] for example, has recently studied the effect of nonmagnetic impurities on the specific heat of superconducting transition metals in the two-band model, assuming a strong-intraband-phonon-coupling limit, and has been able to explain the two-slope behavior of the specific heat of niobium, observed by Shen *et al.*[9]

Guided by these successes, we extend the SMW[1] two-band model to study the thermal conductivity of superconducting transition metals as a function of temperature, using the Green's-function formulation. The effect of nonmagnetic impurities on thermal conductivity is also determined. Starting from the Kubo formula for thermal conductivity, we use the technique employed by Ambegaokar *et al.*[10] The calculations are carried out on the assumption of a strong-intraband-phonon-coupling limit. We make use of the 4×4 matrix formulation of the Green's function, which becomes diagonal in the above coupling limit.[4]

In Sec. II we write the Hamiltonian and other basic equations of the two-band model.[4] In Sec. III an expression for the thermal conductivity K has been derived using the matrix Green's-functions given in Sec. II. This is followed by a discussion of the results of numerical computation and a comparison with the recent experiment of Anderson *et al.*[11] on niobium.